Design Optimization of Single-Layer Antireflective Coating for GaAs$_{1-x}$P$_x$/Si Tandem Cells With x = 0, 0.17, 0.29, and 0.37

Sabina Abdul Hadi, Tim Milakovich, Mayank T. Bulsara, Sueda Saylan, Marcus S. Dahlem, Eugene A. Fitzgerald, and Ammar Nayfeh

Abstract—Single-layer antireflective coating (SLARC) materials and design for GaAs$_{1-x}$P$_x$/Si tandem cells were analyzed by TCAD simulation. We have shown that optimum SLARC thickness is a function of bandgap, thickness, and material quality of top GaAs$_{1-x}$P$_x$ subcell. Cells are analyzed for P fractions x = 0, 0.17, 0.29, and 0.37, and ARC materials: Si$_3$N$_4$, SiO$_2$, ITO, HfO$_2$, and Al$_2$O$_3$. Optimum ARC thickness ranges from 65–75 nm for Si$_3$N$_4$ and ITO to ∼100–110 nm for SiO$_2$. Optimum ARC thickness increases with increasing GaAs$_{1-x}$P$_x$ absorber layer thickness and with decreasing P fraction x. Simulations show that optimum GaAs$_{1-x}$P$_x$ absorber layer thickness is not a strong function of ARC material, but it increases from 250 nm for x = 0 to ∼1 μm for x = 0.29 and 0.37. For all P fractions, Si$_3$N$_4$, HfO$_2$, and Al$_2$O$_3$ performed almost equally, while SiO$_2$ and ITO resulted in ∼1% and ∼2% lower efficiency, respectively. Optimum SLARC thickness increases as the material quality of the top cell increases. The effect of ARC material decreases with decreasing GaAs$_{1-x}$P$_x$ material quality. The maximum efficiencies are achieved for cells with ∼1-μm GaAs$_{0.71}$P$_{0.29}$ absorber (τ = 10 ns): ∼26.57% for 75-nm Si$_3$N$_4$ SLARC and 27.62% for 75-nm SiO$_2$/60-nm Si$_3$N4 double-layer ARC.

Index Terms—Antireflective coating (ARC), Al$_2$O$_3$, GaAs$_{1-x}$P$_x$, HfO$_2$, III–V on Si, ITO, Si$_3$N$_4$, SiO$_2$, Synopsys, TCAD, transfer matrix method (TMM).

I. INTRODUCTION

THE PERFORMANCE of solar cells can be greatly improved with optimized antireflective coating (ARC) that reduces the amount of reflected incident light. Uncoated crystalline silicon (c-Si) surface (refractive index n ∼ 3.7) at interface with air (n ∼ 1) is shown to reflect between 31%–48% of incident light [1]. The concepts of optimum ARC material, number of layers, layer thickness, and surface texturing are continually being studied [1]–[7]. Ideally, the ARC should be abundant material, easily deposited, transparent to most of the solar spectrum, and compatible with materials and processes commonly used in the solar cell industry.

Single-layer ARC (SLARC) can minimize reflection at one specific wavelength [quarter-wave (QW) ARC]. However, the remaining part of the solar spectrum is highly reflected. Hence, for optimum solar cell operation, SLARC is used to minimize wavelength with highest spectral intensity. Double and multilayer ARCs can minimize reflection for more than one wavelength of interest, but the choice of the ARC materials is more constricted, due to refractive index constraints [2]–[4]. Different materials, such as SiO$_2$, SiO$_x$, SiN$_x$, Si$_3$N$_4$, ZnO, ZnS, ITO, TiO$_2$, MgF$_2$/ZnS, etc., have been shown to have good ARC properties [1]–[7], but their performance depends on ARC design and solar cell application. Furthermore, reflectance can be greatly reduced by surface patterning, which is of most interest for concentrated solar cells with normal light incidence [2].

With growing development of tandem cell applications for high efficiency, ARC design specifically tuned to optimize multijunction (MJ) cell performance is needed. Subcells can be grown on top of each other, or they can be fabricated separately and mechanically bonded. Theoretically, optimal efficiency of two junction solar cell can be achieved if bottom cell bandgap E$_g$ is 1.1 eV, while bandgap of top cell is 1.7 eV [8]. Therefore, Si (E$_g$ = 1.12 eV)-based tandem cells with top GaAs$_{1-x}$P$_x$ cell (E$_g$ = 1.42 − 2.22 eV for x = 0 − 1) are an attractive area of research for low cost MJ solar cells.

Main challenges for GaAs$_{1-x}$P$_x$/Si tandem cell are lattice and thermal expansion mismatch between Si and GaAs$_{1-x}$P$_x$ compounds. Nonetheless, high-quality GaAs solar cells were successfully grown on Si by using SiGe step-graded buffers in order to grow virtual Ge substrate that is latticed matched to GaAs [9], [10]. Furthermore, Ge fraction in step-graded buffers can be tuned to lattice match desired GaAs$_{1-x}$P$_x$ compound [11], [12]. Unfortunately, due to its optical properties and decreasing bandgap, SiGe buffer layer would absorb light intended for bottom Si cell [13]–[15]. Another successful way to grow a defect-free III–V layer on silicon is based on the use of a GaP nucleation layer, followed by GaAs$_{1-x}$P$_x$-graded buffer [16]–[19]. The method that would avoid use of graded buffer layers and its related optical losses is mechanical stacking of two subcells. In this paper, we present simulation of the structure that represents mechanically bonded GaAs$_{1-x}$P$_x$ and Si cells.

For optimum performance of MJ cells, current generated in all subcells needs to match. The subcell with the lowest optically generated current limits the current flow in the tandem cell,

decreasing its overall efficiency. Hence, ARC for Si-based MJ cells should be designed to maximize optical absorption in Si base cell but also to not impair the performance of the top cell significantly.

In this paper, we analyze the design requirements for the GaAs$_{1-x}$P$_x$/Si tandem cell for x = 0, 0.17, 0.29, and 0.37 in terms of optimum GaAs$_{1-x}$P$_x$ absorber layer thickness and SLARC. Analysis is carried out for five different ARC materials, i.e., Si$_3$N$_4$, SiO$_2$, ITO, HfO$_2$, and Al$_2$O$_3$, which were chosen either based on their optical compatibility with GaAsP, their common use in a PV application, or convenience of the *in-situ* growth. Transfer matrix method (TMM) is used to estimate the range of optimum antireflective layer thicknesses, which are then analyzed by optical and electrical simulations using TCAD Synopsys [20]–[22]. Finally, results for the optimized GaAs$_{1-x}$P$_x$/Si tandem cell with optimum SLARC design are compared with the equivalent cell with optimized SiO$_2$/Si$_3$N$_4$ double-layer antireflective coating (DLARC) [4], [23].

II. METHODOLOGY

Various ARC materials were analyzed to observe how well they satisfy QW film condition. TMM is then used to estimate SLARC thickness d with minimum reflection for Air/ARC/GaAs$_{1-x}$P$_x$/Si interface with varying GaAs$_{1-x}$P$_x$ thickness, without taking into consideration the light absorption in each layer. In order to account for absorption and to find optimum ARC design for tandem cell, d is further varied in TCAD simulations. Moreover, GaAs$_{1-x}$P$_x$ layer thickness t is varied in order to find optimum tandem cell design with matching subcell currents. GaAs$_{1-x}$P$_x$/Si tandem cell is simulated for top cell thickness t and ARC thickness d for varying GaAs$_{1-x}$P$_x$ minority carrier lifetime τ in order to find an optimum tandem cell design with maximum efficiency. Moreover, the efficiency of the tandem cell is used to identify the optimum design that can be achieved. The efficiency is a performance parameter that encapsulates effects of all variables in this analysis, such as ARC material, ARC thickness, GaAs$_{1-x}$P$_x$ absorber layer thickness, and lifetime. Finally, by means of TCAD simulations, SiO$_2$/Si$_3$N$_4$ DLARC is optimized for the most efficient GaAsP/Si tandem cell and compared with optimum SLARC design.

A. Selection of Single-Layer Antireflective Coating Materials

QW films are specially designed to reduce or completely eliminate reflection at the interface between two media of different refractive indexes n. In our ARC selection process, the QW condition was analyzed for Air (n$_{Air}$ ∼ 1)/GaP (n$_{GaP}$ ∼ 3) and Air/GaAs (n$_{GaAs}$ ∼ 3.4) interfaces, as shown in (1) below [24], since the QW condition for GaAs$_{1-x}$P$_x$ compounds should fall in between

$$n_{ARC} = \sqrt{n_{Air} \cdot n_{GaAs_{1-x}P_x}}. \quad (1)$$

Fig. 1 shows refractive indexes of selected ARC materials, QW conditions for GaAs/Air and GaP/Air interfaces (optical properties utilized from [25]), and solar spectral irradiance AM1.5 [26]. Optical parameters of GaAs$_{1-x}$P$_x$ are obtained by measurements by J. A. Woollam Co. of MOCVD grown
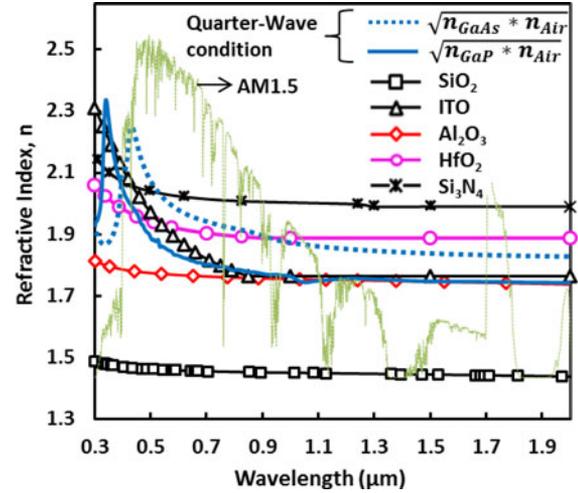

Fig. 1. Refractive indexes of analyzed ARC materials [25], in addition to QW conditions for Air/GaAs and Air/GaP interfaces and solar spectral irradiance AM1.5 (arbitrary units) [26].

2-μm-thick GaAs$_{1-x}$P$_x$ layers on graded SiGe buffer [27]. In terms of reflection, SiO$_2$ performs poorly for the entire wavelength range, and it is included in our further study due to its good surface passivation properties and DLARC applications [4], [23]. For wavelengths with highest spectral intensity ($\lambda \sim$ 400–600 nm), Si$_3$N$_4$, ITO, and HfO$_2$ satisfy the QW condition for GaAs$_{1-x}$P$_x$ compounds the best, while Al$_2$O$_3$ is close to the QW condition of the Air/GaP interface.

B. Transfer Matrix Method

TMM is used to calculate the incident wave reflection with wavelength λ, propagating through multiple layers with refractive index n_i and thickness d_i without accounting for absorption in each medium. Wave transfer matrix used to describe propagation of the wave through homogenous ith layer is defined in (2) below, and transfer matrix describing reflectance at the boundary of two layers with different refractive indexes n$_i$ and n$_{i+1}$ is given in (3) below [24]:

$$M_{\text{prop\_}i} = \begin{bmatrix} e^{-j\varphi_i} & 0 \\ 0 & e^{j\varphi_i} \end{bmatrix}, \quad \varphi_i = n_i d_i \frac{2\pi}{\lambda} \quad (2)$$

$$M_{i/i+1} = \frac{1}{2 \cdot n_{i+1}} \begin{bmatrix} n_{i+1}+n_i & n_{i+1}-n_i \\ n_{i+1}-n_i & n_{i+1}+n_i \end{bmatrix}. \quad (3)$$

Wave propagating through N layers, assuming $N+1$ boundaries (sandwiched between two infinite media), can be described by matrix M, which is given in [24]

$$M = \begin{bmatrix} A & B \\ C & D \end{bmatrix} = \prod_{i=1}^{N} (M_{i-1/i} M_{\text{prop\_}i} M_{i/i+1}). \quad (4)$$

Total intensity reflectance of wave propagation through N layers, from infinite region with n_0 to infinite region with n$_{N+1}$ is then equal to [24]

$$R_{0,N+1} = \left| -\frac{C}{D} \right|^2. \quad (5)$$
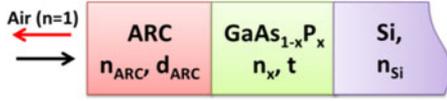
Fig. 2. Schematics of the TMM structure used in order to estimate optimum ARC for GaAs$_{1-x}$P$_x$ tandem cell.
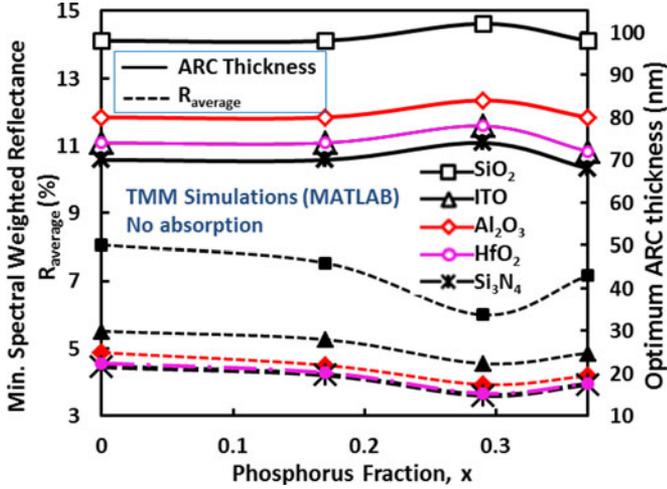
Fig. 3. Minimum average weighted reflectance, $R_{average}$ (%) as a function of P fraction x for different ARC material. GaAs$_{1-x}$P$_x$ thickness with minimum Raverage shown above is equal to 2, 0.8, 2 (1.3 for SiO$_2$), and 1 μm for x = 0, 0.17, 0.29, and 0.37, respectively.

Fig. 2 shows schematics of TMM applied to ARC optimization for GaAs$_{1-x}$P$_x$/Si tandem cell.

In order to find optimum SLARC thickness, reflectance intensity at each wavelength R$_{0,N+1}$ (λ), is weighted by normalized spectrum intensity I(λ) and averaged over the spectrum, as shown in

$$R_{average} = \frac{1}{\lambda_{end} - \lambda_{start}} \int_{\lambda_{start}}^{\lambda_{end}} R_{0,N+1}(\lambda) \cdot I(\lambda) d\lambda. \quad (6)$$

The solar spectrum range from λ_{start} = 300 nm to λ_{end} = 1100 nm is taken into consideration since GaAs$_{1-x}$P$_x$ and Si optical responsively fall within it. Analysis is repeated for varying GaAs$_{1-x}$P$_x$ thickness and P fractions of x = 0, 0.17, 0.29, and 0.37. Fig. 3 shows minimum average spectral weighted reflectance, $R_{average}$ as a function of P fraction (x), for each analyzed ARC material. GaAs$_{1-x}$P$_x$ thickness with minimum $R_{average}$ varied with x and was equal to 2, 0.8, 2 (1.3 for SiO$_2$), and 1 μm for x = 0, 0.17, 0.29, and 0.37, respectively.

When absorption is not taken into account, optimum ARC thickness ranges roughly between 65 and 85 nm for all tested fractions of x and ARC materials, with the exception of SiO$_2$. HfO$_2$. and Si$_3$N$_4$, show the lowest reflectance over the analyzed spectrum range (3.6%). Si$_3$N$_4$ requires least ARC thickness to achieve minimum reflectance and is closely followed by HfO$_2$.

SLARC thickness with minimum average reflectance over the entire solar spectrum is selected for further device simulations in TCAD.
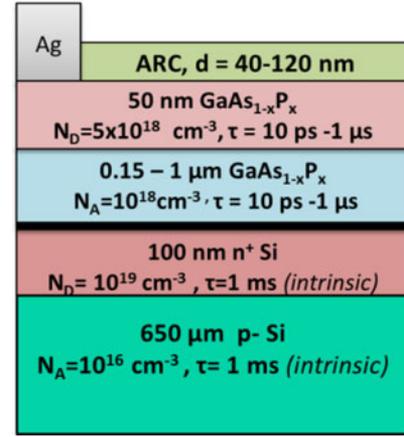

Fig. 4. Schematic cross section of GaAs$_{1-x}$P$_x$/Si tandem cell simulated in TCAD.

C. TCAD Simulation Model

Sentaurus TCAD by Synopsys [20]–[22] is used for electrical and optical simulation of the solar cell devices. Synopsys tools Sentaurus Structure Editor, Sentaurus Device (SDevice), and Inspect are used.

GaAs$_{1-x}$P$_x$/Si tandem cells are simulated for different ARC materials with varying ARC and GaAs$_{1-x}$P$_x$ thickness, as well as the GaAs$_{1-x}$P$_x$ lifetime. Complex refractive indexes for ARC materials, GaAs and Si are used from [25], while optical parameters of GaAs$_{1-x}$P$_x$ (x = 0.17 − 0.37) are obtained by measurements of MOCVD grown 2-μm-thick epi layer [27].

The Si solar cell is optimized such that the absorber is 650-μm-thick lightly doped p-type Si substrate (N$_A$ = 10^{16} cm^{-3}) and the heavily doped (N$_D$ = 10^{19} cm^{-3}) 100-nm-thick n-type emitter. GaAs$_{1-x}$P$_x$ top cell is designed with variable absorber thickness and acceptor doping N$_A$ = 10^{18} cm^{-3} and 50-nm thick emitter with N$_D$ = 5 × 10^{18} cm^{-3}. The lifetime τ of Si is modeled as doping dependent in the Physics section of the SDevice Synopsys tool, and its intrinsic value is set to 1 ms, which is consistent with the high-quality c-Si wafer [28]–[30]. The GaAs$_{1-x}$P$_x$ lifetime is modeled as a fixed value, and it is varied from 10 ps to 1 μs, which is the range of values reported for GaAs epi growth on SiGe-graded buffers [31] and pure GaAs materials [32]. The values for the energy bandgap for GaAs$_{1-x}$P$_x$ are utilized from [33], while for Si and GaAs, default values from TCAD are used. The tunnel diode between two cells is simulated as a very thin highly conductive region [34]. Optical and resistive losses in the tunnel junction are not taken into consideration in these simulations. The effect of interface surface recombination is also ignored. Fig. 4 shows a schematic cross section of the simulated solar cell.

By increasing the P fraction, the bandgap of the top GaAs$_{1-x}$P$_x$ cell increases from ~1.43 eV for x = 0 to ~1.88 eV for x = 0.37 [33], resulting in lower photogenerated current in the top cell. In order to achieve matching currents of subcells, the optimum GaAs$_{1-x}$P$_x$ absorber layer thickness, as well as the optimum SLARC thickness, changes with increasing P fraction. Consequently, optimum SLARC thickness and
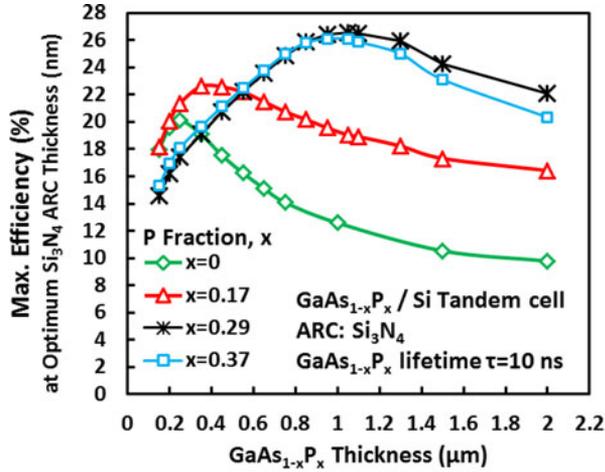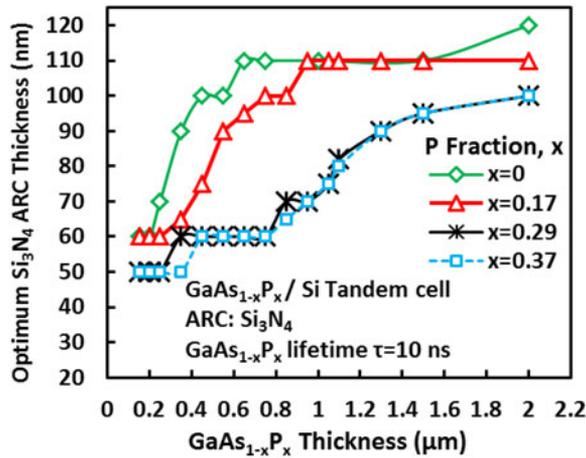
Fig. 5.   (a) Maximum efficiency of $GaAs_{1-x}P_x$/Si tandem cell. (b) Optimum Si_3N_4 ARC thickness (nm) as a function of $GaAs_{1-x}P_x$ absorber layer thickness for x = 0, 0.17, 0.29, and 0.37 and $GaAs_{1-x}P_x$ lifetime $\tau = 10$ ns.

material will differ from the values estimated by TMM analysis that did not take into consideration the absorption or the tandem cell specific requirement for matching subcell currents.

III. RESULTS AND DISCUSSION

In order to show the effect of the P fraction on the optimum SLARC and $GaAs_{1-x}P_x$ absorber layer thickness, TCAD simulations were carried out for Si_3N_4 as a fixed ARC material, based on TMM results (as shown in Fig. 3). Fig. 5(a) shows the maximum efficiency of the $GaAs_{1-x}P_x$ tandem cell as a function of the $GaAs_{1-x}P_x$ absorber layer thickness at optimum Si_3N_4 ARC thickness for x = 0, 0.17, 0.29, and 0.37, with the $GaAs_{1-x}P_x$ lifetime $\tau = 10$ ns. The $GaAs_{1-x}P_x$ absorber layer thickness for maximum efficiency increases from 250 nm for x = 0 to ∼1 μm for x = 0.29 and 0.37. The tandem cell for x = 0.29 performs the best with maximum efficiency ∼26.57%, closely followed by cells with x = 0.37.

Fig. 5(b) shows values for optimum Si_3N_4 ARC thickness at which maximum efficiency is achieved for the varying $GaAs_{1-x}P_x$ absorber layer thickness and the P frac-
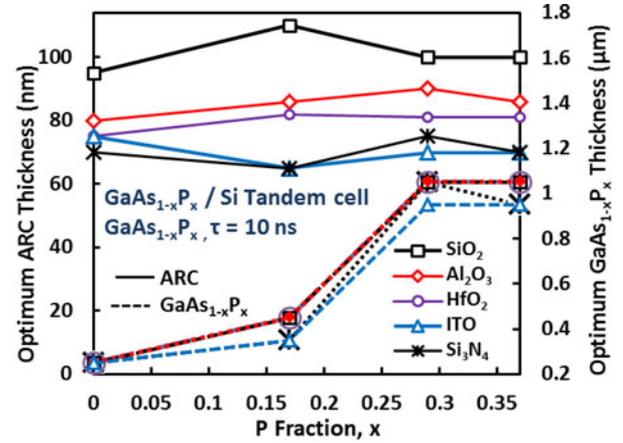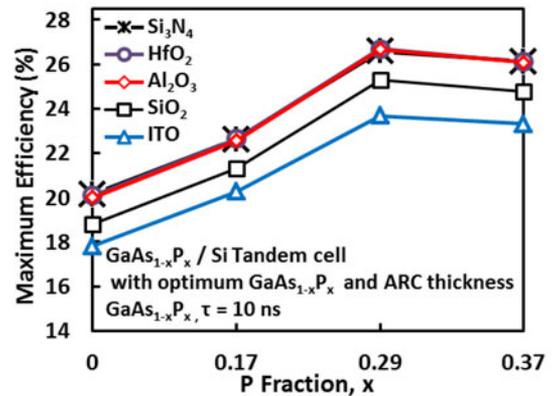

Fig. 6.   (a) Optimum SLARC thickness for optimum $GaAs_{1-x}P_x$ absorber layer thickness for different ARC materials. (b) Maximum efficiency as a function of P fraction x for optimized $GaAs_{1-x}P_x$/Si tandem cells with $GaAs_{1-x}P_x$ lifetime $\tau = 10$ ns.

tion x. The maximum overall efficiency for all P fractions was achieved for Si_3N_4 thickness in the range between 65 and 75 nm. However, optimum ARC thickness increases with increasing $GaAs_{1-x}P_x$ absorber layer thickness. This is due to the fact that more light is absorbed in the top cell with a thicker absorber layer, and photogeneration in the bottom Si cell needs to be enhanced by favoring longer wavelengths. Furthermore, the trend in Fig. 5(b) shows that the generally thicker ARC layer is required for cells with lower P fraction (x = 0 and 0.17). This is due to the fact that cells with lower bandgap absorb more of the solar spectrum; therefore, the ARC thickness needs to be tuned such that performance of the bottom cell is maximized. Similar analysis was repeated for other ARC materials. Optimum ARC thickness as a function of P fraction (x) and its corresponding optimum $GaAs_{1-x}P_x$ absorber layer thickness for different ARC materials are shown in Fig. 6(a) for the lifetime $GaAs_{1-x}P_x = 10$ ns. Fig. 6(b) shows maximum efficiency as a function of the P fraction for $GaAs_{1-x}P_x$/Si tandem cells with optimized ARC and $GaAs_{1-x}P_x$ absorber layer thicknesses.

The results in Fig. 6 show that optimum SLARC thickness is smallest for Si_3N_4 and ITO (65–75 nm) and largest for SiO_2 (∼100–110 nm). The optimum top absorber thickness is mostly
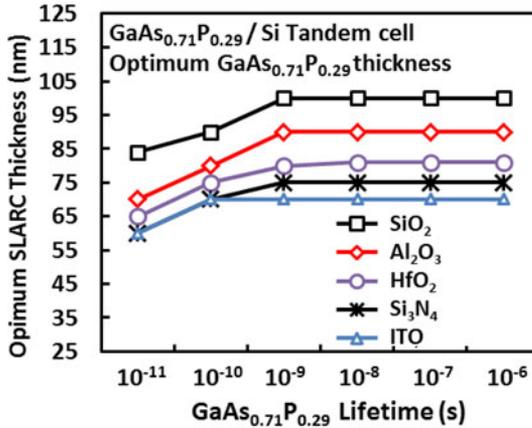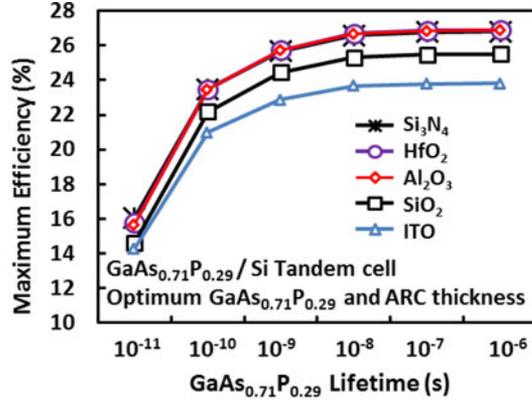
Fig. 7. (a) Maximum efficiency. (b) Optimum SLARC thickness as a function of GaAs$_{0.71}$P$_{0.29}$ minority carrier lifetime τ for GaAs$_{0.71}$P$_{0.29}$/ Si tandem cell with optimum GaAs$_{0.71}$P$_{0.29}$ absorber thickness.

unchanged with respect to different ARC materials, with the exception of ITO that resulted in slightly thinner GaAs$_{1-x}$P$_x$ layer. In terms of efficiency, for all P concentrations, Si$_3$N$_4$, HfO$_2$, and Al$_2$O$_3$ performed almost equally, while SiO$_2$ and ITO resulted in ∼1% and ∼2% lower efficiency, respectively. With respect to ARC performance and optimum thickness, TCAD simulations are in agreement with TMM results (see Fig. 3), except for ITO, which was outperformed by SiO$_2$. This is probably the result of larger absorption in ITO compared with SiO$_2$, due to its higher extinction coefficients k [25].

We have shown that optimum SLARC thickness changes with changing GaAs$_{1-x}$P$_x$ absorber layer, because of the change in photogenerated current of both subcells. Similarly, optimum SLARC thickness changes with GaAs$_{1-x}$P$_x$ material quality, which, in this study, is represented by minority carrier lifetime τ. Optimum SLARC and GaAs$_{1-x}$P$_x$ absorber layer thickness were studied for 10 ps ≤ L τ ≤ 1 μs. Since x = 0.29 resulted in highest efficiency (for GaAs$_{1-x}$P$_x$ absorber layer thickness between 950–1 μm), the effect of GaAs$_{1-x}$P$_x$ lifetime is shown here for that specific P fraction.

Fig. 7(a) shows maximum efficiency of GaAs$_{0.71}$P$_{0.29}$/Si tandem cell with optimized top cell absorber and ARC thicknesses, as a function of τ. The advantage of Si$_3$N$_4$, Al$_2$O$_3$, and HfO$_2$
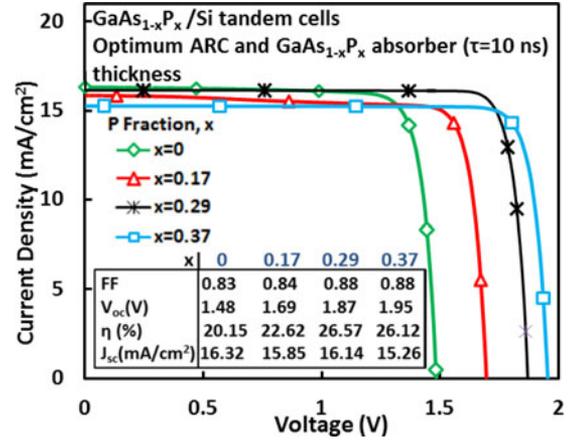

Fig. 8. J–V characteristics of GaAs$_{1-x}$P$_x$/Si tandem cells (x = 0, 0.17, 0.29, and 0.37) with optimum SLARC and GaAs$_{1-x}$P$_x$ absorber layer thicknesses with GaAs$_{1-x}$P$_x$ lifetime equal to 10 ns.
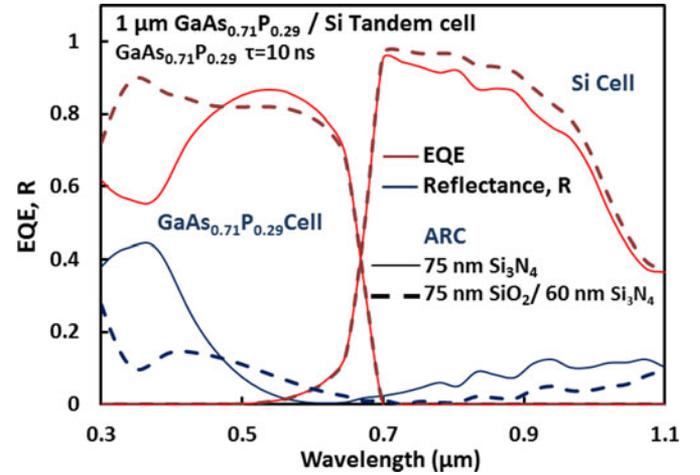

Fig. 9. EQE (red) and reflectance (blue) curves for 1-μm GaAs$_{0.71}$P$_{0.29}$/Si tandem cell with 75-nm Si$_3$N$_4$ SLARC (full line) and 75-nm SiO$_2$/60-nm Si$_3$N$_4$ DLARC (dashed line). The GaAs$_{0.71}$P$_{0.29}$ lifetime equals 10 ns.

materials decreases with lower material quality, with efficiency gain ranging from ∼1.5% at 10 ps to ∼3% at 1 μs when compared with ITO. Fig. 7(b) shows optimum ARC thickness as a function of τ for GaAs$_{0.71}$P$_{0.29}$/Si tandem cell with optimum top cell absorber thickness. Optimum ARC thickness increases as the material quality of the top cell increases, in an attempt to enhance photogeneration in the bottom cell. Similarly, for poor lifetime in the top cells, ARC thickness decreases in favor of optical generation in the top cell. The same trend is observed for all ARC materials and all P fractions (not shown here).

Fig. 8 shows J–V characteristics of the GaAs$_{1-x}$P$_x$/Si tandem cells (x = 0, 0.17, 0.29, and 0.37) with optimum SLARC and GaAs$_{1-x}$P$_x$ absorber layer thicknesses with the GaAs$_{1-x}$P$_x$ lifetime equal to 10 ns. It can be noted that the fill factor of cells with x = 0.29 and x = 0.37 is slightly higher, due to the better match between subcell currents.

The best performing cell with a 1-μm-thick GaAs$_{0.71}$P$_{0.29}$ absorber is further improved by using the optimized 75-nm SiO$_2$/60-nm Si$_3$N$_4$ DLARC. Fig. 9 shows a comparison of
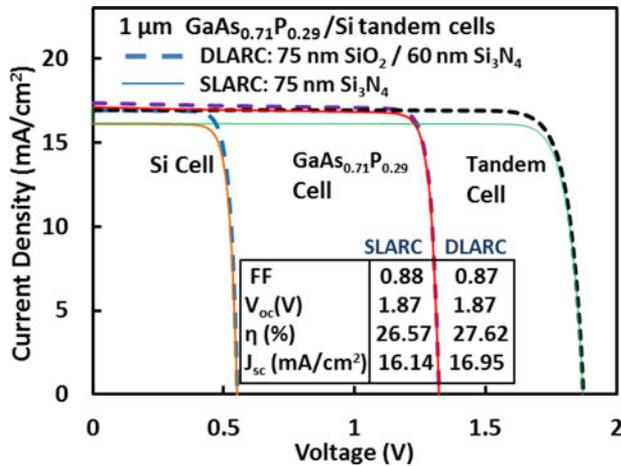
Fig. 10. J–V characteristics $GaAs_{0.71}P_{0.29}/Si$ of top, bottom and tandem cell for 75-nm Si_3N_4 SLARC (full lines), and 75-nm SiO_2/60-nm Si_3N_4 DLARC (dashed lines). $GaAs_{0.71}P_{0.29}$ lifetime equals to 10 ns.

reflectance and external quantum efficiency (EQE) for a 1-μm-thick $GaAs_{0.71}P_{0.29}/Si$ tandem cell with 75-nm Si_3N_4 SLARC and 75-nm SiO_2/60-nm Si3N4 DLARC. By using optimized SiO_2/Si_3N_4 DLARC, overall reflectance is decreased (for $\lambda = 300 - 450$ nm and $\lambda > 700$ nm). This results in improved spectral response of both cells, resulting in higher J_{sc} and ~1% efficiency gain, as shown in Fig. 10.

IV. Conclusion

In summary, a simulation study was carried out in order to find the optimum ARC material and thickness for $GaAs_{1-x}P_x/Si$ tandem cells. Optimum SLARC thickness is smallest for Si_3N_4 and ITO (65–75 nm) and largest for SiO_2 (~100–110 nm). However, optimum ARC thickness increased with increasing $GaAs_{1-x}P_x$ absorber layer thickness. Furthermore, a thicker ARC layer is required for cells with lower P fraction (x = 0 and 0.17). The optimum $GaAs_{1-x}P_x$ absorber layer thickness increases from 250 nm for x = 0 to ~1 μm for x = 0.29 and 0.37. Maximum efficiency of ~ 26.57% was achieved for cells with x = 0.29 with optimized SLARC (75 nm Si_3N_4) and absorber layer thickness (~1 μm). For all P fractions, maximum efficiency was achieved for 65–75-nm-thick Si_3N_4 SLARC. Finally, efficiency for the ~1-μm $GaAs_{0.71}P_{0.29}/Si$ tandem cell is increased to 27.62% by using optimized 75-nm SiO_2/60-nm Si3N4 DLARC.

References

[1] Y. Matsumoto, J. A. Urbano, M. Ortega, E. Barrera, and G. Romero-Paredes, "Towards cost-effective antireflective-coating and surface-texturing," in *Proc. IEEE 38th Photovoltaic Spec. Conf.*, Austin, TX, USA, 2012, pp. 000258–000264.

[2] J. Zhao, A. Wang, X. Dai, M. A. Green, and S. R. Wenham, "Improvements in silicon solar cell performance," in *Proc. IEEE 22nd Photovoltaic Spec. Conf.*, Las Vegas, NV, USA, 1991, pp. 399–402.

[3] A. Al-Bustani and M. Y. Feteha, "Design of antireflection coatings for triple heterojunction AlGaAs-GaAs space solar cells," in *Proc. IEEE Workshop High Perform. Electron Devices Microw. Optoelectron. Appl.*, 1995, pp. 55–60.

[4] K. A. Abade, F. J. Fonseca, R. D. Mansano, and P. Abade Jr., "PECVD single-layer (SiN:H) and double-layer (SiN:H/SiO$_2$) ARC on mono and multicrystalline silicon solar cells," in *Proc. IEEE Photovoltaic Spec. Conf.*, 2000, pp. 307–310.

[5] D. N. Wright, E. S. Marstein, and A. Holt, "Double layer anti-reflective coatings for silicon solar cells," in *Proc. IEEE 31st Photovoltaic Spec. Conf.*, 2005, pp. 1237–1240.

[6] M. Neander, F. Gromball, D. Neumann, N. P. Harder, and W. A. Nositschka, "Anti-reflective-coating tuned for higher solar module voltage," in *Proc. IEEE 4th World Conf. Photovoltaic Energy Convers.*, 2006, pp. 2070–2072.

[7] D. Bouhafsa, A. Moussia, A. Chikouchea, and J. M. Ruizb, "Design and simulation of antireflection coating systems for optoelectronic devices: Application to silicon solar cells," *Sol. Energy Mater. Sol. Cells*, vol. 52, nos. 1/2, pp. 79–93, Mar. 1998.

[8] S. R. Kurtz, P. Faine, and J. M. Olson, "Modeling of two-junction, series-connected tandem solar cells using top cell thickness as an adjustable parameter," *J. Appl. Phys.*, vol. 68, pp. 1890–1895, 1990.

[9] J. A. Carlin, M. K. Hudait, S. A. Ringel, D. M. Wilt, E. B. Clark, C. W. Leitz, M. Currie, T. Langdo, and E. A. Fitzgerald, "High efficiency GaAs-on-Si solar cells with high V_{oc} using graded GeSi Buffers," in *Proc. IEEE 28th Photovoltaics Spec. Conf.*, 2000, pp. 1006–1011.

[10] C. L. Andre, D. M. Wilt, A. J. Pitera, M. L. Lee, E. A. Fitzgerald, and S. A. Ringel, "Impact of dislocation densities on n+/p and p+/n junction GaAs diodes and solar cells on SiGe virtual substrates," *J. Appl. Phys.*, vol. 98, no. 1, pp. 014502-1–014502-5, 2005.

[11] A. Nayfeh, "Heteroepitaxial growth of relaxed germanium on silicon," Ph.D. dissertation, Dept. Elect. Eng., Stanford Univ., Stanford, CA, USA, 2006.

[12] A. K. Okyay, M Cengiz Onbasli, B. Ercan, H.-Y. Yu, S. Ren, D. A. B. Miller, K. C. Saraswat, and A. M. Nayfeh, "High efficiency monolithic photodetectors for integrated optoelectronics in the near infrared," in *Proc. IEEE LEOS Annu. Meeting Conf.*, Oct. 4–8, 2009, pp. 303–304.

[13] S. Abdul Hadi, P. Hashemi, N. DiLello, A. Nayfeh, and J. L. Hoyt, "Effect of c-Si$_{1-x}$Ge$_x$ thickness grown by LPCVD on the performance of thin-film a-Si/c-Si$_{1-x}$Ge$_x$/c-Si heterojunction solar cells," *MRS Proc.*, vol. 1447, pp. mrss12–1447-v01–09, 2012.

[14] S. Abdul Hadi, P. Hashemi, N. DiLello, A. Nayfeh, and J. L. Hoyt, "Thin film a-Si/c-Si$_{1-x}$Ge$_x$/c-Si heterojunction solar cells with Ge content up to 56%," in *Proc. IEEE 38th Photovoltaic Spec. Conf.*, 2012, pp. 5–8.

[15] S. Abdul Hadi, P. Hashemi, N. DiLello, E. Polyzoeva, A.Nayfeh, and J. L. Hoyt, "Thin-film Si$_{1-x}$Ge$_x$ HIT solar cells," *Sol. Energy*, vol. 103, pp. 154–159, May 2014.

[16] K. Hayashi, T. Soga, H. Nishikawa, T. Jimbo, and M. Umeno, "MOCVD growth of GaAsP on Si for tandem solar cell applications," in *Proc. 1st World Conf. Photovoltaic Energy Convers.*, 1994, pp. 1890–1893.

[17] J. F. Geisz, J. M. Olson, M. J. Romero, C. S. Jiang, and A. G. Norman, "Lattice-mismatched GaAsP solar cells grown on silicon by OMVPE," in *Proc. IEEE 4th World Conf. Photovoltaic Energy Convers.*, 2006, pp. 772–775.

[18] S. A. Ringel, J. A. Carlin, T. J. Grassman, B. Galiana, A. M. Carlin, C. Ratcliff, D. Chmielewski, L. Yang, M. J. Mills, A. Mansouri, S. P. Bremner, A. Ho-Baillie, X. Hao, H. Mehrvarz, G. Conibeer, and M. A, Green, "Ideal GaP/Si heterostructures grown by MOCVD: III-V/active-Si subcells, multijunctions, and MBE-to-MOCVD III-V/Si interface science," in *Proc. IEEE 39th Photovoltaic Spec. Conf.*, FL, USA, 2013, pp. 3383–3388.

[19] K. N. Yaung, J. R. Lang, and M. L. Lee, "Towards high efficiency GaAsP solar cells on (001) GaP/Si," in *Proc. IEEE 40th Photovoltaic Spec. Conf.*, 2014, pp. 0831–0835.

[20] TCAD: Process and device Simulation Tools, World Wide Web. [Online]. Available: http://www.synopsys.com/Tools/TCAD/Pages/default.aspx

[21] S. Abdul Hadi, A. Nayfeh, P. Hashemi, and J. L. Hoyt, "A-Si/c-Si$_{1-x}$Ge$_x$/c-Si heterojunction solar cells," in *Proc. Conf. Simul. Semicond. Processes Devices*, 2011, pp. 191–194.

[22] S. Abdul Hadi, P. Hashemi, A. Nayfeh, and J. L. Hoyt, "Thin film a-Si/c-Si$_{1-x}$Ge$_x$/c-Si heterojunction solar cells: Design and material quality requirements," *ECS Trans.*, vol. 41, no. 4, pp. 3–14, 2011.

[23] B. Conrad, T. Zhang, A. Lochtefeld, A. Gerger, C. Ebert, M. Diaz, L. Wang, I. Perez-Wurfl, and A. Barnett, "Double layer antireflection coating and window optimization for GaAsP/SiGe tandem on Si," in *Proc. IEEE 40th Photovoltaic Spec. Conf.*, 2014, pp. 1143–1147.

[24] B. E. A. Saleh and M. C. Teich, "Photonic-crystal optics," in *Fundamentals of Photonics*, 2nd ed. Hoboken, NJ, USA: Wiley, 2007, ch. 7, sec. 1, pp. 246–252.

[25] S. Semilab, N-k database. [Online]. Available: Web: http://www.sopra-sa.com, 2013.

[26] Reference Solar Spectral Irradiance Air Mass AM1.5. [Online]. Available:http://rredc.nrel.gov/solar/spectra/am1.5/, 2013.

[27] Optical properties of MOCVD grown GaAs$_{1-x}$P$_x$ graded buffers, measured by J. A. Woollam Co. [to be published].

[28] J. E. Park, D. K. Schroder, S. E. Tan, B. D. Choi, M. Fletcher, A. Buczkowski, and F. Kirscht, "Silicon epitaxial layer lifetime characterization," *J. Electrochem. Soc.*, vol. 148, no. 8, pp. G411–G419, 2001.

[29] A. Nayfeh, V. Koldyaev, P. Beaud, M. Nagoga, and S. Okhonin, "A leakage current model for SOI based floating body memory that includes the Poole-Frenkel effect," in *Proc. IEEE SOI Conf.*, vol. 75, pp. 75–76, 2008.

[30] S. Abdul Hadi, P. Hashemi, N. DiLello, E. Polyzoeva, A. Nayfeh, and J. L. Hoyt, "Effect of germanium fraction on the effective minority carrier lifetime in thin film amorphous-Si/crystalline-Si$_{1-x}$Ge$_x$/crystalline-Si heterojunction solar cells," *AIP Advances*, vol. 3, no. 5, pp. 052119-1–052119–6, 2013.

[31] C. L. Andre, J. J. Boeckl, D. M. Wilt, A. J. Pitera, M. L. Lee, E. A. Fitzgerald, B. M. Keyes, and S. A. Ringel, "Impact of dislocations on minority carrier electron and hole lifetimes in GaAs grown on metamorphic SiGe substrates," *Appl. Phys. Lett.*, vol. 84, no. 18, pp. 3447-3449, 2004.

[32] Properties of GaAs. [Online]. Available: http://www.ioffe.ru/SVA/NSM/Semicond/GaAs/electric.html, 2013.

[33] G. D. Pitt and C. E. E. Stewart, "The electrical properties of GaAs$_{1-x}$P$_x$ alloys from a high-pressure experiment," *J. Phys. C, Solid State Phys.*, vol. 8, p. 1397, 1975.

[34] *Simulation of a GaAs/GaInP dual-junction solar cell*, Synopsys Inc., (2012). [Online]. Available: https://solvnet.synopsys.com.

Authors' photographs and biographies not available at the time of publication.